Desalination and Water Treatment
www.deswater.com
doi: 10.1080/19443994.2015.1043589

57 (2016) 11337–11347
May

Taylor & Francis
Taylor & Francis Group

Synthesis of $NiFe_2O_4$ using degreasing cotton as template and its adsorption capacity for Congo Red

Chao Kong, Jia Li*, Futian Liu, Yi Song, Peng Song

School of Material Science and Engineering, University of Jinan, Jinan, China, Tel. +86 15552877599; email: kc1989kc@163.com (C. Kong), Tel. +86 13953185430; email: mse_lij@ujn.edu.cn (J. Li), Tel. +86 13708924960; email: mse_liuft@ujn.edu.cn (F. Liu), Tel: +86 15288874553; email: 370460183@qq.com (Y. Song), Tel: +86 15254135506; email: 854242610@qq.com (P. Song)

Received 30 September 2014; Accepted 10 April 2015

ABSTRACT

In this contribution, the biomorphic $NiFe_2O_4$ was synthesized by using degreasing cotton as template via a simple one-step process involving impregnation and calcination. The obtained samples were characterized by X-ray diffraction patterns (XRD), scanning electron microscope (SEM), alternating gradient magnetometer and nitrogen adsorption–desorption isotherms. It was found that the as-prepared samples retained the characteristic hollow fiber morphology of the degreasing cotton template, and were composed of $NiFe_2O_4$ nanoparticles with the grain size ranging from 5 to 20 nm. The Brunauer Emmett Teller (BET) specific surface area and pore volume of the obtained sample were 118.620 $m^2 g^{-1}$ and 0.303 $cm^3 g^{-1}$, respectively. In addition, the Congo red (CR) adsorption performances of the obtained samples were also evaluated. The effects of calcination temperature and pH on CR adsorption were discussed. The results showed that the best adsorption performance (89.45 mg g^{-1}) was obtained when the calcination temperature was 600°C. The process of CR adsorption was spontaneous, exothermic and favorable, and was well described by both the Langmuir isotherm model and the pseudo-second-order kinetics model. The obtained sample was effective in adsorbing CR in the neutral and acidic conditions. Electrostatic attraction between samples and CR molecules was the main reason of the high adsorption.

Keywords: Degreasing cotton; Biotemplate; Spinel ferrite; Adsorption; Congo red

1. Introduction

Dyes are widely used mostly in the textiles, paper, plastics, leather, food and cosmetic industry to color products [1]. Due to their large-scale production and extensive application, dyes have turned into serious pollutants, leading to environmental problems, especially public health problems [2]. Many organic dyes are poisonous and harmful to human beings. Therefore, the toxic dyes should be removed before discharged into the environment [3]. The removal of dyes from wastewater is becoming a research hotspot attracting more and more attentions around the world. Many methods have been developed to remove the dyes from aqueous environment, such as photocatalysis [4], oxidation [5], biodegradation [6], Fenton [7] and adsorption [8].

The adsorption technology is widely used in the field of wastewater treatment. A large number of absorbents have been investigated by previous studies such as activated carbon [9], chitosan [10], synthetic

*Corresponding author.

resins [11], layered double hydroxide [12]. Some of these adsorbents are restricted from widespread application because of their high cost, difficult disposal and regeneration. In addition, the separation of these adsorbents from wastewater is still a problem. In order to overcome the problem, many separation techniques have been applied, such as centrifugation, membrane filtration and magnetic separation. Among these methods, magnetic separation may be an ideal choice owing to its high-efficiency. It is beneficial to their recycle from wastewater in magnetic field using magnetic absorbent. There have been a lot of reports published using various types of magnetic absorbents [13–15]. In particular, the MFe_2O_4 (M = Mn, Co, Ni, Zn) ferrites with spinel structure have been used as absorbent due to their magnetic properties [1,16]. $NiFe_2O_4$, as a member of ferrites family, also has potential applications in magnetic materials and absorbent materials.

The aim of this work is to report the synthesis and characterization of biomorphic $NiFe_2O_4$ and its Congo red (CR) adsorption performance. Biotemplate method was used in the preparation of $NiFe_2O_4$ in the present study. The biotemplate method always adopts biological materials which provide variety of structures at micro and nanometric scale [17]. Due to the biological material with its unique structural diversity, hierarchical pore structure, renewable capability, easy to remove and no environmental pollution, the biotemplate method can be a very effective approach to prepare adsorption materials.

In this experiment, the biomorphic $NiFe_2O_4$ was synthesized from degreasing cotton template via a simple process involving impregnation and calcination. Compared with previous preparation methods of $NiFe_2O_4$, the preparation of $NiFe_2O_4$ from degreasing cotton template was more facile and effective. In addition, the biomorphic $NiFe_2O_4$ from degreasing cotton template had higher surface area and recovery efficiency in water than $NiFe_2O_4$ powders obtained from conventional preparation methods. Then, the as-prepared $NiFe_2O_4$ was used as adsorbent to remove CR from aqueous solution by batch adsorption process. The influences of processing parameters, the adsorption kinetics and thermodynamics were investigated in detail.

2. Experimental

2.1. Sample preparation

In this article, $NiFe_2O_4$ with biomorphic structure was prepared using degreasing cotton (Tai'an Jinzhong Health Materials Co.) as template. The chemicals, $Ni(NO_3)_2{\cdot}6H_2O$, $Fe(NO_3)_3{\cdot}9H_2O$ and NaOH were analytic grade reagents. A typical synthetic procedure was as followed: 5 g degreasing cotton were submerged in the 100 mL mixture solution of 0.5 M $Ni(NO_3)_2{\cdot}6H_2O$ and 0.5 M $Fe(NO_3)_3{\cdot}9H_2O$ for 24 h. The impregnated samples were then dried in air at 80°C for 2 h, and were subsequently calcined in air at temperatures between 500 and 700°C for 1 h. The designations of the as-prepared samples are shown in Table 1.

Table 1
Designation of the as-prepared samples

Sample	Fe:Ni ratio (at %)	Calcination temperature (°C)
NFO500	2:1	500
NFO600	2:1	600
NFO700	2:1	700

2.2. Characterization

The crystallographic structure of sample was characterized by X-ray diffraction patterns (XRD with Cu $K\alpha$ radiation source; $\lambda = 0.15406$ nm, Scan span: 5–90°; Model D8-Advance, Germany). The morphologies and chemical compositions of the samples were observed by scanning electron microscope (SEM, FEI QNANTA FEG 250, United States) equipped with energy-dispersive X-ray spectrometer (EDS, Model INCA Energy 3294, Oxford, UK). The functional group of samples was analyzed by Fourier transform infrared spectrometer (FTIR, Nicolet670, Thomas Nicolet, America). The magnetic properties were investigated by MicroMag 2900 AGM (alternating gradient magnetometer, Princeton Measurements Corporation, USA). A 722 UV–vis spectrophotometer was used for determination of CR concentration at 488 nm in the solutions. The pore structure of the obtained sample was analyzed by nitrogen adsorption–desorption at 77 K on a surface area analyzer (ASAP2020M+C, Micrometrics, GA, USA). The surface area of sample was evaluated by the Langmuir model and Brunauer Emmett Teller (BET) model, while the pore size distribution (PSD) was estimated by Barrett–Joyner–Halenda (BJH) theory.

2.3. Adsorption experiments

The adsorptive removal of CR (chemical formula: $C_{32}H_{22}N_6Na_2O_6S_2$, FW = 696.68, $\lambda_{max} = 488$ nm) by the obtained sample adsorbent was studied by batch adsorption experiments at room temperature, where 50 mg of the obtained adsorbent and 100 mL of the

CR solutions (10–150 mg L^{-1}) were added. The stock solution of CR (1 g L^{-1}) was prepared in distilled water and desired concentrations of CR were obtained by diluting the stock solution with distilled water. The calibration curve of CR was prepared by measuring the absorbance of different predetermined concentrations of the samples at λ_{max} = 488 nm using UV–vis spectrophotometer. Then the concentrations of the solutions were determined by plotting the calibration curve of CR with a linear regression equation. The changes in the absorbance of all solution samples were presented and determined at certain time intervals during the adsorption process. The amount of adsorbed CR q_e (mg g^{-1}) was calculated based on a mass balance equation was given below:

$$q_e = \frac{(C_0 - C_e) \times V}{W} \quad (1)$$

where q_e (mg g^{-1}) is the equilibrium adsorption capacity per gram dry weight of the adsorbent; C_e (mg L^{-1}) is the equilibrium concentration of CR solution; C_0 (mg L^{-1}) is the initial concentration of CR solution; V (L) is the volume of the solution; W (g) is the mass of the adsorbent. Further, at t time, the quantity of adsorbed CR q_t (mg g^{-1}) was calculated by:

$$q_t = \frac{(C_0 - C_t) \times V}{W} \quad (2)$$

where C_t (mg L^{-1}) is the CR concentration at t time. Then, kinetic studies and adsorption thermodynamics were carried out on the adsorption of CR by the obtained samples.

3. Results and discussion

3.1. Characterization of $NiFe_2O_4$

Fig. 1 shows the XRD patterns of samples calcinated at different temperatures. All the diffraction peaks could be indexed to the cubic spinel structure of nickle ferrite according to JCPDS card No. 54-0964. Further, the XRD patterns revealed the monophasic formation and good crystalline nature of $NiFe_2O_4$. The sharpness of the X-ray diffraction peaks confirmed that $NiFe_2O_4$ was highly crystallized without any other impurities. The average grain sizes of $NiFe_2O_4$ at 500, 600 and 700˚C were calculated to be 5.81, 15.94 and 21.90 nm from the full-width at half maximum of (311) peak according to Scherrer's formula [18], respectively. It demonstrated that the crystal size of $NiFe_2O_4$ increased gradually with the increasing temperature.

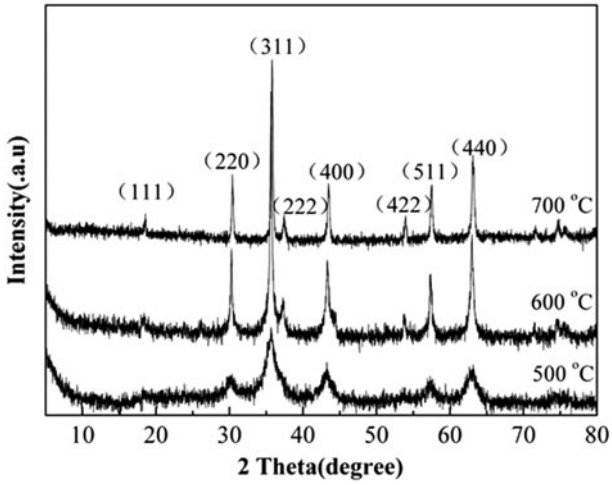

Fig. 1. XRD patterns of the as-prepared samples at different calcination temperatures.

To obtain further evidence that degreasing cotton really acted as a template to produce fiber structure, the degreasing cotton and obtained sample were analyzed by SEM, respectively. The surface of the cotton fibers was smooth and the diameter was about between 8 and 15 μm (Fig. 2(a)). Compared with the raw template, the obtained sample retained the original morphology of degreasing cotton (Fig. 2(b)–(f)). And most of the obtained biomorphic sample fibers were hollow. The magnified images in Fig. 2(c)–(f) showed that these hollow fibers were composed of uniformly distributed nanoparticles and were about 5–10 μm in diameter. The EDS spectrum in the inset of Fig. 2(f) indicates that these particles are composed of Ni, Fe and O. Combining with the above XRD results, it could be deduced that the hollow fibers were composed of $NiFe_2O_4$ nanoparticles.

Moreover, it was found that the average diameter of fibers decreased from 10 to 5 μm as the temperature increased from 500 to 700˚C. This might be attributed to the more shrinkage of the degreasing cotton fibers at higher temperature. Furthermore, comparing Fig. 2(c) and (e), it can be seen that the grain size of the obtained sample increased with increasing temperature, which was in agreement with the above XRD results.

The N_2 adsorption–desorption measurement and the corresponding BJH PSDs of the obtained biomorphic samples are revealed in Fig. 3. The isotherms of the obtained samples (Fig. 3(a)) were featured by a distinct hysteresis loop in the desorption process in a comparatively high relative pressure range. Moreover, the adsorption and the desorption curve overlapped at low relative pressures ($P/P_0 < 0.4$). This indicated

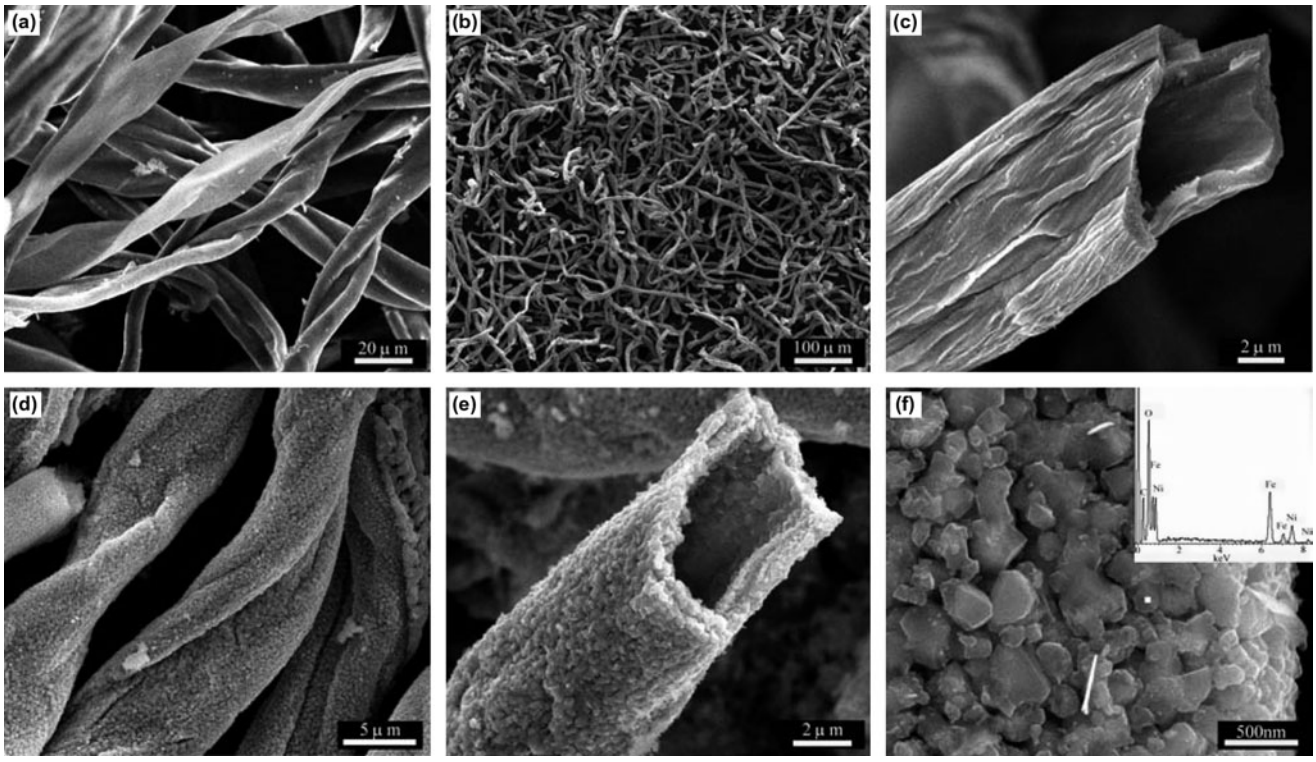

Fig. 2. SEM images of the original degreasing cotton (a) and SEM images of the obtained biomorphic $NiFe_2O_4$ at different calcination temperatures: 500℃ (b)–(c) and 700℃ (d)–(f).

that the obtained biomorphic samples possessed a large number of mesoporous texture. The corresponding PSD plots upon the BJH method showed in Fig. 3(b). In particular, the PSD of NFO600 displayed a obvious peak in the mesoporous range, but the samples of NFO500 and NFO700 had a wide pore distribution with weak and unclear peaks. The surface area and the pore volume of different samples were summarized in Table 2. Compared with the three samples, NFO500 exhibited the highest surface area (133.96 $m^2\ g^{-1}$). The specific surface area of NFO600 was 118.63 $m^2\ g^{-1}$ and it had the biggest pore volume (0.303 $cm^3\ g^{-1}$).

Since the obtained biomorphic samples used to be absorbents and the magnetic properties of magnetic absorbents directly influenced the callback efficiency, AGM was used to measure the magnetic properties of them at room temperature with a maximum applied field of 10,000 Oe. As displayed in Fig. 4, the synthesized biomorphic sample showed the typical ferromagnetic behavior. The saturation magnetizations (M_S) of the sample was 45.577 emu g^{-1} and the coercive forces (H_C) of it was 202.208 Oe, which indicated that the prepared sample with mid-hard magnetism could be used as a reusable absorbent for fast, convenient, and highly efficient removal of dyes from the wastewater, as shown the inset in Fig. 4.

3.2. Adsorption capacities of the as-prepared samples

The adsorption capacities of the as-prepared samples for CR are given in Fig. 5(a). The high experimental q_e was obtained when the calcination temperature was 600℃. Fig. 5(a) also indicated that the adsorption capacity increased rapidly at the primary stage and the change range became smaller until the adsorption equilibrium was reached.

Fig. 5(b) shows the UV–vis spectrum changes of adsorption process for CR on the sample NFO600 at different adsorption times and the structure of CR. It displayed that the CR solution exhibited three absorption peaks at 499, 345 and 236 nm, respectively. Among them, the peak at 499 nm was corresponding to chromophore structure next to the azo agent. The bands in the ultraviolet region located at 236 and 345 nm were attributed to the benzoic and naphthalene rings. As revealed in Fig. 5(b), with the increase of adsorption time, all the absorption peaks went down to a certain extent synchronously. When the adsorption time reached 24 h, the adsorption peak

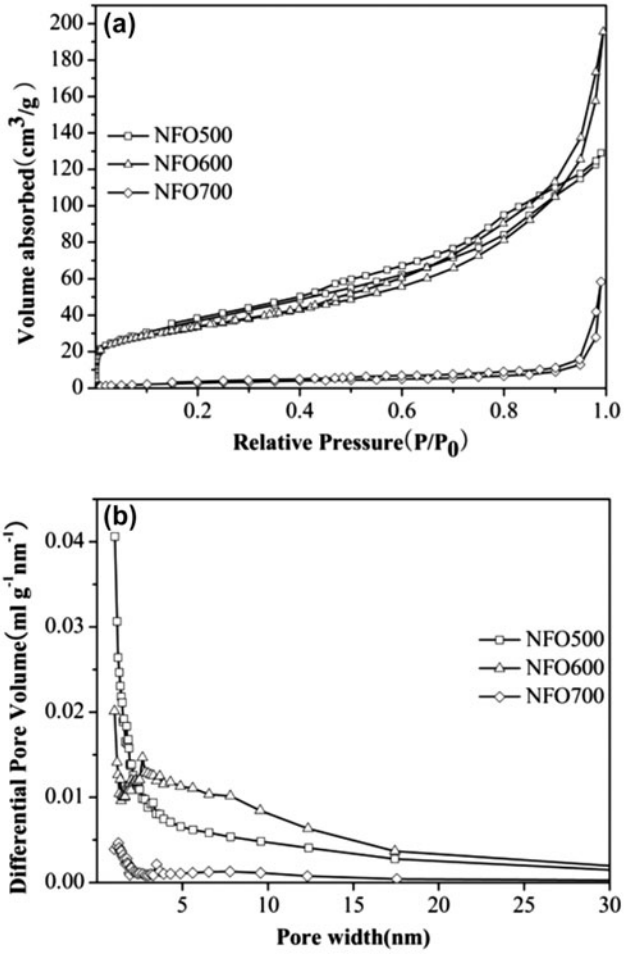

Fig. 3. Low-temperature N_2 adsorption–desorption isotherms of the three samples (a) and corresponding pore size distribution curves (b).

Table 2
Pore structural parameters of the as-prepared samples

Sample	BET surface area ($m^2\ g^{-1}$)	Pore volume ($cm^3\ g^{-1}$)
NFO500	133.96	0.200
NFO600	118.62	0.303
NFO700	11.67	0.090

at 499 nm almost disappeared. The results indicated that CR molecules in solution were adsorbed on the as-prepared sample.

3.3. Adsorption kinetics

The pseudo-first-order and pseudo-second-order model are used to interpret the adsorption experiment

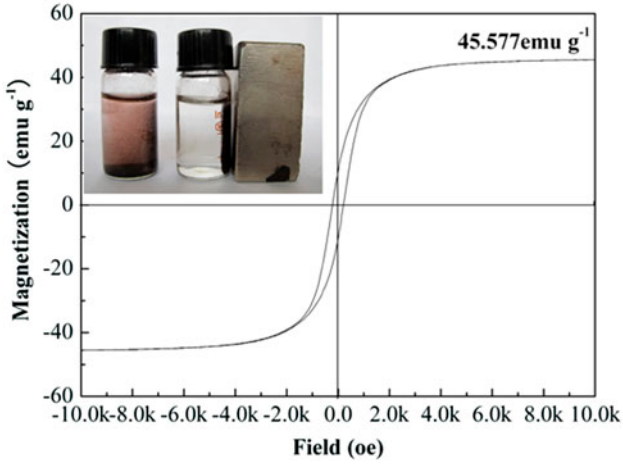

Fig. 4. AGM curves of the obtained NFO600 at room temperature and the photo showing magnetic separation.

data. The pseudo-first-order kinetic model [19] is defined as:

$$\frac{1}{q_t} = \frac{1}{q_{1e}} + \frac{k_1}{q_{1e}}\left(\frac{1}{t}\right) \tag{3}$$

where t is the adsorption time, q_t is the amount of dye adsorbed per unit of adsorbent (mg g^{-1}) at time t, k_1 is the pseudo-first-order rate constant (min^{-1}), q_{1e} is the equilibrium adsorption. The adsorption rate constant (k_1) was obtained from the plot of q_t^{-1} vs t^{-1}.

Ho and McKay [20] presented the pseudo-second-order kinetic as:

$$\frac{t}{q_t} = \frac{1}{k_2 q_{2e}^2} + \frac{1}{q_{2e}}t \tag{4}$$

where k_2 is the pseudo-second-order rate constant (g mg^{-1} min^{-1}). The q_{2e} and k_2 can be calculated by linear plot of $t\ q_t^{-1}$ against t.

Fig. 6 shows the plots of the pseudo-first-order and the pseudo-second-order kinetics of CR adsorption on the as-prepared samples. The calculated kinetic parameters are given in Table 3. The comparison of correlation coefficients (R^2) of the two models reflected that the adsorption process did not follow the pseudo-first-order kinetic model, and the calculated value (q_{1e}) obtained from this equation did not give reasonable value, which was much lower than experimental data. On the contrary, all the R^2 values obtained from pseudo-second-order model were close to unity, indicating that the adsorption of CR fitted well to this model. The calculated q_{2e} were ranged

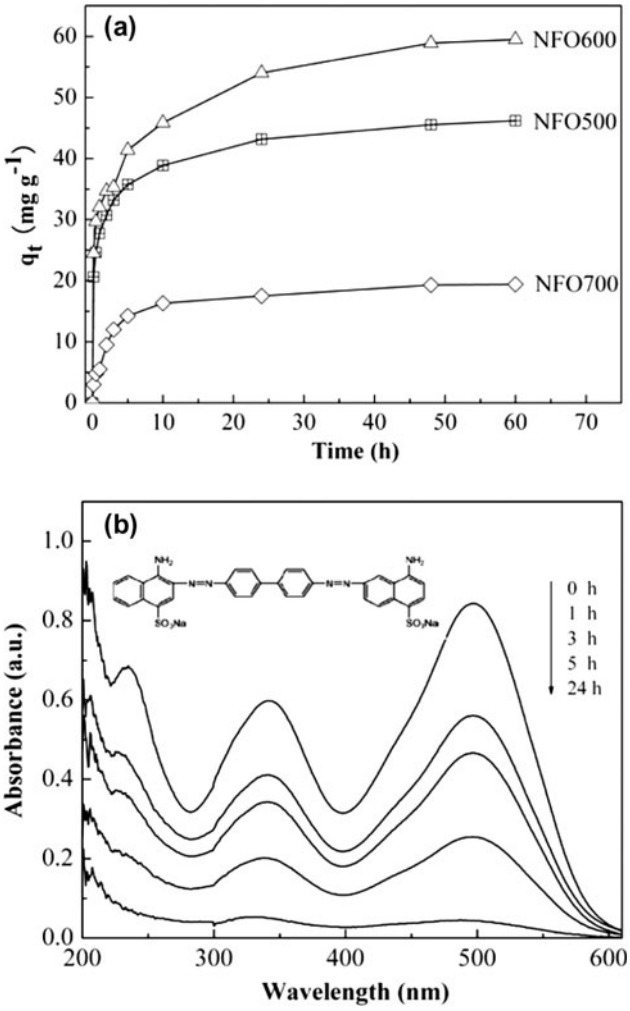

Fig. 5. Adsorption capacities of the as-prepared samples (a), and UV–vis spectrum of CR adsorption on the NFO600 sample (b). (CR: 100 mL 50 mg L^{-1}, adsorbent dosage 50 mg, neutral pH, room temperature: 30°C.)

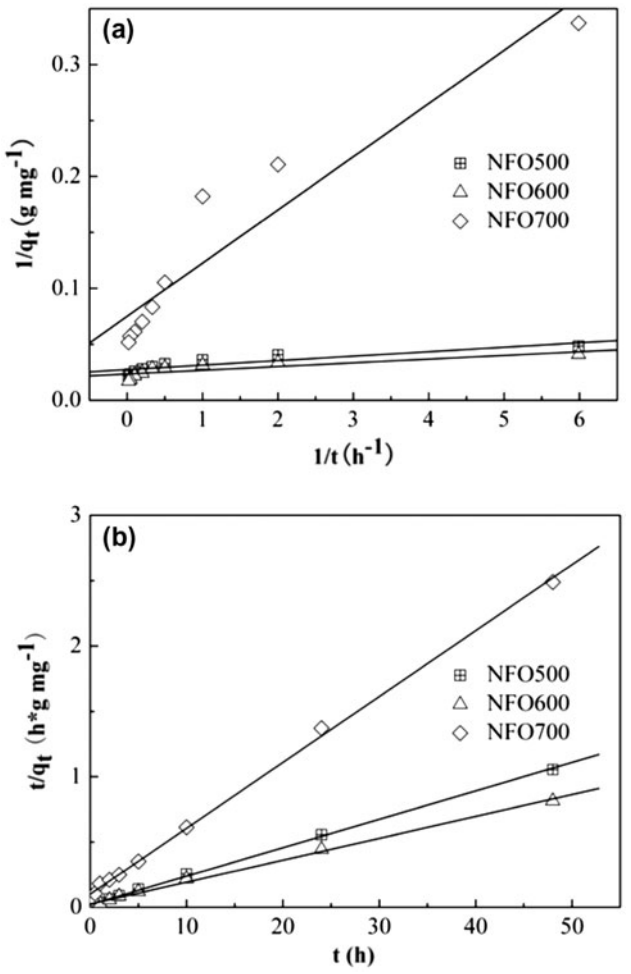

Fig. 6. Adsorption kinetic for adsorption of CR on the as-prepared samples pseudo-first order (a), and pseudo-second order (b).
Notes: Adsorption conditions for CR:100 mL of 50 mg L^{-1} of dye, adsorbent dosage 50 mg, neutral pH, room temperature: 30°C.

from 8.2 to 59.6 mg g^{-1}. NFO600 sample had the maximum adsorption capacity. This could be explained that the NFO600 had relatively large surface area and the biggest pore volume, ensured that NFO600 had more adsorption active sites and higher adsorption efficiency.

3.4. Adsorption isotherms

To simulate the adsorption isotherm, two conventional used models, the Langmuir [21] and Freundlich [22] isotherms Eqs. (5) and (6), were employed to analyze how CR molecules interacted with the surface of the as-prepared samples.

$$\frac{C_e}{q_e} = \frac{1}{q_{max} k_L} + \frac{C_e}{q_{max}} \tag{5}$$

$$\log q_e = \log k_F + \frac{1}{n} \log C_e \tag{6}$$

where q_e (mg g^{-1}) is the adsorption capacity at equilibrium, C_e (mg L^{-1}) is the equilibrium concentration of CR, q_{max} (mg g^{-1}) is the maximum adsorption capacity of the as-prepared samples, and k_L (L mg^{-1}) is a constant related to the ability of adsorption. And the values of k_L and q_{max} could be determined from the slope and intercept of the linear plot C_e/q_e against C_e (Fig. 7(a)). k_F (mg$^{1-1/n}$ L$^{1/n}$ g^{-1}) is the Freundlich

Table 3
Adsorption parameters got from kinetic for the adsorption of 50 mg L^{-1} CR on the as-prepared samples

	Pseudo-first-order			Pseudo-second-order		
Sample	q_{1e} (mg g^{-1})	k_1 (min^{-1})	R^2	q_{2e} (mg g^{-1})	k_2 (min^{-1})	R^2
NFO500	36.6166	0.1468	0.7954	45.977	0.0225	0.9987
NFO600	42.7533	0.1419	0.7020	59.6303	0.0113	0.9961
NFO700	13.3422	0.6343	0.9016	19.8333	0.0253	0.9983

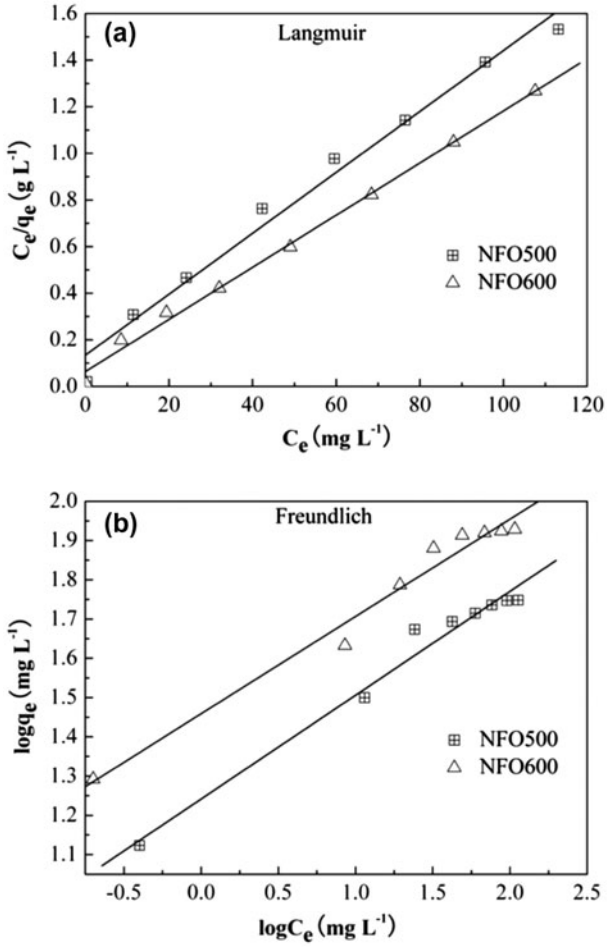

Fig. 7. Adsorption isotherms for adsorption of CR on the as-prepared samples: the Langmuir model (a) and the Freundlich model (b).
Note: Adsorption conditions for CR: 100 mL of CR dye, adsorbent dosage 50 mg, neutral pH, room temperature: 30℃.

equilibrium constant indicative of adsorption. The values of k_F and n could be calculated from the plot of lg q_e vs lg C_e (Fig. 7(b)).

Table 4 gives the adsorption parameters values calculated from the Langmuir and Freundlich isothermal models. The calculated regression coefficients R^2 from Langmuir isotherm models were much higher than the values from Freundlich isotherm models, meaning that the Langmuir isotherm models was better fit with the experimental data. The CR covering on the as-prepared samples surface was of the Langmuir type. Thus, it was reasonable to suggest that the adsorption of CR on the obtained samples was site-specific and monolayer.

Table 5 compares the adsorption capacities of the obtained samples with different types of adsorbents [1,15,23–26]. $NiFe_2O_4$ ferrites used in this study had considerable higher q_{max} values. More importantly, the simplicity of the preparation method and magnetic separation made $NiFe_2O_4$ ferrites better used in the adsorption for CR.

3.5. Adsorption thermodynamics

In order to discuss the effect of temperature on the adsorption capacity, the adsorption studies were carried out at five temperatures (30, 40, 50, 60, and 70℃). From Fig. 8(a), it was observed that the adsorption capacity decreased from 60.3 to 37.1 mg g^{-1} when the temperature increased from 30 to 70℃, indicating the exothermic nature of the adsorption reaction. The thermodynamic parameter related to the adsorption process, were calculated by the following equation [27]:

$$\Delta G^0 = -RT \ln K_\alpha \tag{7}$$

$$\ln K_\alpha = \frac{\Delta S^0}{R} - \frac{\Delta H^0}{RT} \tag{8}$$

$$K_\alpha = \frac{C_0}{C_e} \tag{9}$$

where R is the universal gas constant (8.314 J mol^{-1} K^{-1}), T is the temperature of the solution (K), K is equilibrium constant, C_0 (mg L^{-1}) is the initial concentration of CR and C_e (mg L^{-1}) is the equilibrium

Table 4
Adsorption parameters from adsorption isotherms for the adsorption of CR on the as-prepared samples

	Langmuir			Freundlich		
Sample	k_L (L mg^{-1})	q_{max} (mg g^{-1})	R_L^2	k_F (L mg^{-1})	n	R_F^2
NFO600	0.1750	89.45	0.9953	28.7627	4.0365	0.9758
NFO500	0.09757	76.51	0.9842	17.4373	3.7817	0.9777

Table 5
Adsorption capacities of CR on various adsorbents

Adsorbents	q_{max} (mg g^{-1})	References
$NiFe_2O_4$	89.45	Present study
$MnFe_2O_4$	92.4	[1]
$CoFe_2O_4$	244.5	[1]
Fe_3O_4	68.5	[15]
Hollow zinc ferrite	16.58	[23]
Hierarchical NiO nanosheets	151.7	[24]
ZrO_2 hollow spheres	59.5	[25]
Chitosan coated magnetic iron oxide	56.66	[26]

concentration of CR. Enthalpy ΔH^0 (kJ mol^{-1}) and entropy ΔS^0 (J mol^{-1} K^{-1}) were calculated from the slope and intercept from the plot of $\ln C_0/C_e$ vs $1/T$ (Fig. 8(b)). The thermodynamic parameters were given in Table 6. The value of ΔH^0 (−20.864 kJ mol^{-1}) was negative, proving the adsorption of CR was an exothermic process. The negative values of ΔG^0 at the temperature range from 30 to 70˚C indicated that the adsorption of CR on NFO600 was spontaneous. In addition, ΔG^0 increased from −2.324 to −1.322 kJ mol^{-1} when temperature increased from 30 to 70˚C, confirming that the adsorption was spontaneous at low temperature. The value of ΔS^0 (−26.018 J mol^{-1} K^{-1}) was negative, suggesting that there was a decrease in the degree of freedom of the adsorption of CR on NFO600. It also indicated that the dye molecules were restricted toward the NFO600 surface, resulting in the decrease of entropy.

3.6. Effect of pH

As an important parameter influencing the adsorption capacity, the solution pH could affect the chemical properties of both dye molecule and the adsorbent. The zeta potentials of NFO600 at various solution pH values were measured and the results are depicted in Fig. 9. The point of zero charge of NFO600 was found at about pH 6.4. Zeta potentials of the sample were gradually reduced with the increasing pH. At pHs below 6.4, zeta potentials were positive, and over the range of pH 6.4–11 they were negative.

The effect of initial solution pH on the CR adsorption was investigated in the pH ranges from 3 to 11. As shown in Fig. 10, CR adsorption capacity of NFO600 increased when pH increased from 3 to 7. When the pH continued to increase, the adsorption capacity decreased rapidly. The maximum adsorption capacity of CR was 75.76 mg g^{-1} at pH 7. The actual maximum adsorption might happen at a certain value in the pH-range of 5–7. Since CR molecule with two sulfonic groups ionized easily in acidic media and became a soluble CR anion. The adsorbent was positively charged in acidic solution (Fig. 9). The excellent adsorption ability could be attributed to the fact that a considerably high electrostatic attraction existed between the adsorbent surfaces and negatively charged CR molecules [28]. So in the pH-range of 3–7, the CR adsorption capacity always maintained a high level. On the other hand, the adsorption capacity decreased slightly at pH 3 and pH 5. This could possibly be attributed to the increase of competition between protonation and the adsorption sites on the surface of NFO600 for CR [15]. In alkaline solution, the negatively charged adsorbent would repulse the negatively charged CR molecules, causing the large reduction in CR adsorption. In addition, an abundance of OH^- ions in alkaline solution existed a competitive environment with anionic ions of CR, which also caused a decrease of CR adsorption [29].

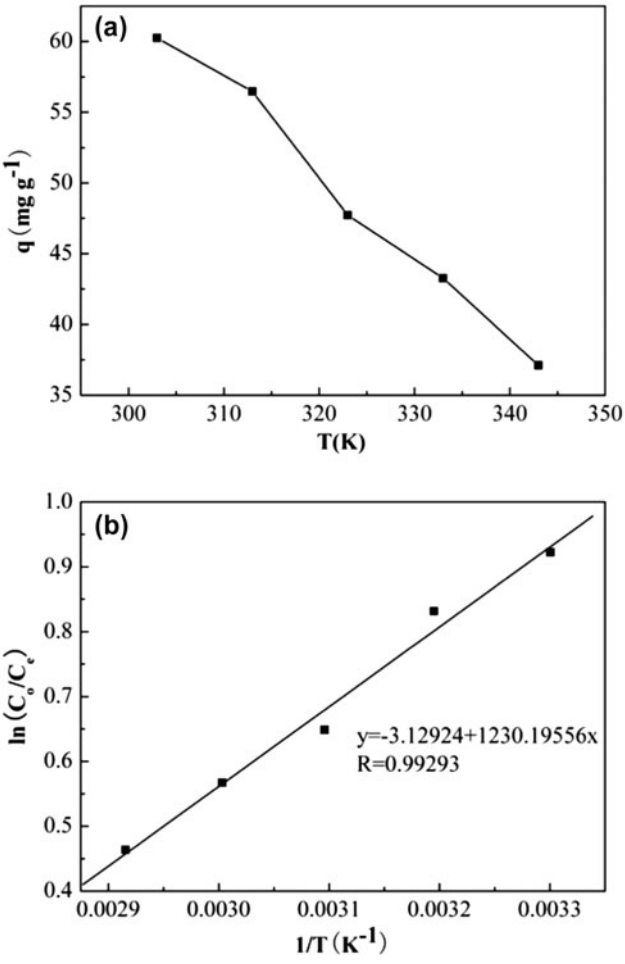

Fig. 8. The adsorption capacity of CR on NFO600 at different temperatures (a) and Van't Hoff plot for the adsorption of the CR on NFO600 (b).
Notes: Adsorption conditions for CR: 100 mL of 50 mg L^{-1} of dye, adsorbent dosage 50 mg, neutral pH.

3.7. Reusability of the as-prepared samples

The reusability efficiency of the adsorbent material is an important factor in the wastewater treatment. For this experiment, five cycles of adsorption/desorption experiments of NFO600 were carried out and the adsorption capacity in each cycle is shown in Fig. 11.

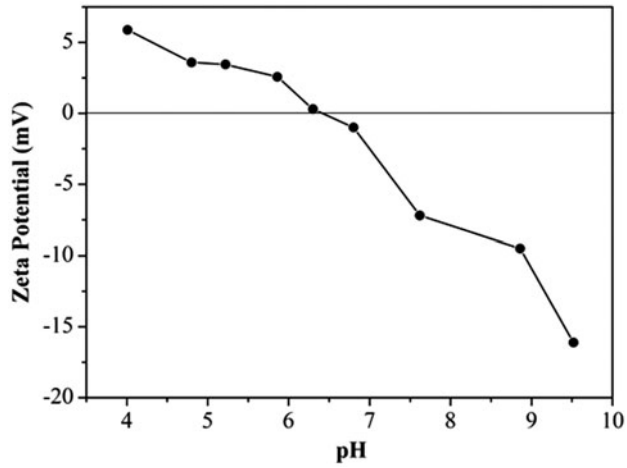

Fig. 9. Zeta potential of NFO600 before adsorption.

After the first cycle, NFO600 was separated from CR solution with a magnet. Then, the sample of NFO600 after CR adsorption was stirred with methanol solution, dried and used for the next removal cycle. It was observed that the adsorption capacity of the recycled sample could still be 46.51 mg g^{-1} in the fifth cycle, as high as 78.70% of the first cycle. Therefore, the as-prepared samples can be used as a reusable magnetic absorbent for the removal of CR.

3.8. Investigation on the adsorption mechanism

CR is acidic dye. In aqueous solution, CR dye dissociates to the sodium ions (Na^+) and the sulfonate anions ($R\text{-}SO_3^-$). The pH_{zpc} (the pH of zero point charge) of the obtained samples is about 6.4. Below the pH_{zpc}, because of protonation, the adsorbent surface is positively charged, the electrostatic attraction with anionic dye molecules occurs, contributing to the high CR adsorption capacity. With the increase pH of CR solution, a proportional decrease in adsorption took place, due to the successive deprotonation of positive charged groups on the adsorbent and the electrostatic repulsion between negatively charged sites on the adsorbent and dye anions. Therefore, we

Table 6
Thermodynamic parameters for the adsorption of CR on $NiFe_2O_4$

			ΔG^0 at temperature(℃) (kJ mol^{-1})				
Dye concentration (mg L^{-1})	ΔH^0 (kJ mol^{-1})	ΔS^0 (J mol^{-1} K^{-1})	30	40	50	60	70
50	−10.228	−26.018	−2.324	−2.164	−1.742	−1.570	−1.322

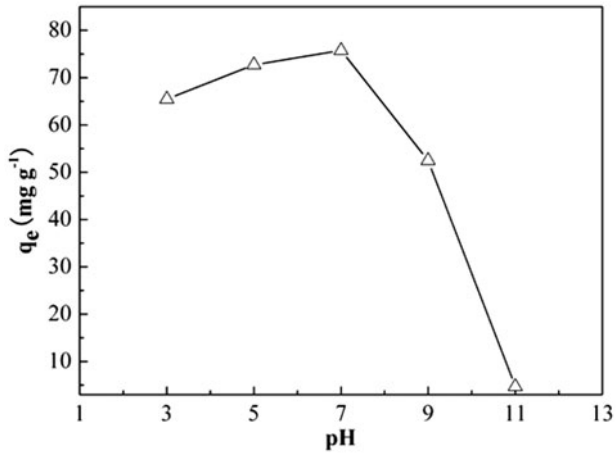

Fig. 10. The effect of initial pH of dye solution on adsorption of CR onto the as-prepared sample.
Notes: Adsorption conditions for CR: 100 mL of 50 mg L^{-1} of dye, adsorbent dosage: NFO600, 50 mg, room temperature: 30°C, adsorption time: 24 h.

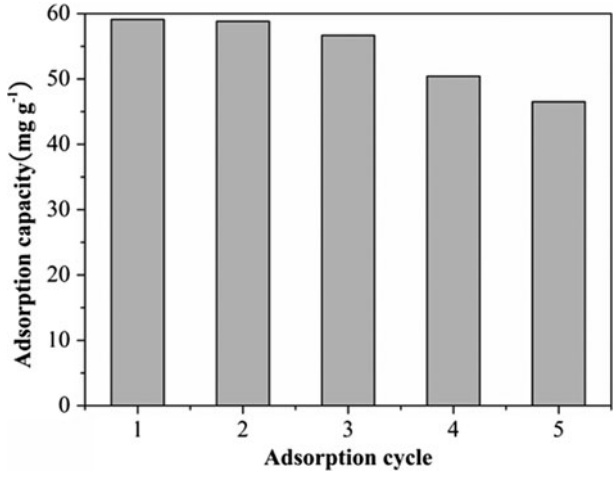

Fig. 11. Performance of reusability of the as-prepared sample.
Notes: Adsorption conditions for CR: 100 mL of 50 mg L^{-1} of dye, adsorbent dosage: NFO600, 50 mg, room temperature: 30°C, adsorption time: 48 h.

can draw a conclusion that the electrostatic attraction between the adsorbent and CR is the primary mechanism for the high CR adsorption. In addition, CR can become adsorbed onto the absorbent surface by the chemical interaction, such as hydrogen bonds, coordination effect between metal ions and amine groups.

4. Conclusions

The biomorphic $NiFe_2O_4$ was successfully synthesized by the biotemplate method as revealed by XRD and SEM. Among the obtained simples synthesized at different conditions, NFO600 had the best adsorption property for CR. The maximum CR adsorption capacity calculated from the Langmuir isotherm model was 89.45 mg g^{-1}. Factors affecting adsorption, such as initial dye concentration, temperature and pH were evaluated. Analysis of adsorption isotherm showed that our adsorption experiment accorded with Langmuir model. The results of adsorption kinetics proved that the adsorption process well fit to the pseudo-second-order kinetic model. Adsorption thermodynamics indicated the CR adsorption on the as-prepared samples was spontaneous and exothermic process. The as-prepared samples had ideal magnetic performance, which favored their high-efficient magnetic separation from wastewater.

Acknowledgments

This work was supported by National Natural Science Foundation of China (Grant No. 51172095) and National Natural Science Foundation of China (Grant No. 61102006).

References

[1] L.X. Wang, J.C. Li, Y.Q. Wang, L.J. Zhao, Q. Jiang, Adsorption capability for Congo red on nanocrystalline MFe_2O_4 (M = Mn, Fe Co, Ni) spinel ferrites, Chem. Eng. J. 181–182 (2012) 72–79.
[2] M. Belhachemi, F. Addoun, Adsorption of congo red onto activated carbons having different surface properties: Studies of kinetics and adsorption equilibrium, Desalin. Water Treat. 37 (2012) 122–129.
[3] M. Iram, C. Guo, Y. Guan, A. Ishfaq, H. Liu, Adsorption and magnetic removal of neutral red dye from aqueous solution using Fe_3O_4 hollow nanospheres, J. Hazard. Mater. 181 (2010) 1039–1050.
[4] J. Fernández, J. Kiwi, C. Lizama, J. Freer, J. Baeza, H.D. Mansilla, Factorial experimental design of Orange II photocatalytic discolouration, J. Photochem. Photobiol. A. 151 (2002) 213–219.
[5] W.X. Chen, W.Y. Lu, Y.Y. Yao, M.H. Xu, Highly efficient decomposition of organic dyes by aqueous-fiber phase transfer and in situ catalytic oxidation using fiber-supported cobalt phthalocyanine, Environ. Sci. Technol. 41 (2007) 6240–6245.
[6] A. Karakaya, Y. Laleli, S. Takaç, Development of process conditions for biodegradation of raw olive mill wastewater by *Rhodotorula glutinis*, Int. Biodeterior. Biodegrad. 75 (2012) 75–82.
[7] M. Munoz, G. Pliego, Application of intensified Fenton oxidation to the treatment of sawmill wastewater, Chemosphere 109 (2014) 34–41.
[8] X. Zhuang, Y. Wan, C.M. Feng, Y. Shen, D. Zhao, Highly efficient adsorption of bulky dye molecules in wastewater on ordered mesoporous carbons, Chem. Mater. 21 (2009) 706–716.

[9] J.L. Sotelo, G. Ovejero, A. Rodríguez, S. Álvarez, J. Galán, J. García, Competitive adsorption studies of caffeine and diclofenac aqueous solutions by activated carbon, Chem. Eng. J. 240 (2014) 443–453.
[10] T.V. Rêgo, T.R.S. Cadaval, G.L. Dotto, L.A.A. Pinto, Statistical optimization, interaction analysis and desorption studies for the azo dyes adsorption onto chitosan films, J. Colloid Interface Sci. 411 (2013) 27–33.
[11] Y. Yu, Y.Y. Zhuang, Z.H. Wang, M.Q. Qiu, Adsorption of water-soluble dyes onto resin NKZ, Ind. Eng. Chem. Res. 42 (2003) 6898–6903.
[12] R.R. Shan, L.G. Yan, K. Yang, S.J. Yu, Y.F. Hao, H.Q. Yu, B. Du, Magnetic Fe_3O_4/MgAl-LDH composite for effective removal of three red dyes from aqueous solution, Chem. Eng. J. 252 (2014) 38–46.
[13] N.J. Wang, L.L. Zhou, J. Guo, Q.Q. Ye, J.M. Lin, J.Y. Yuan, Adsorption of environmental pollutants using magnetic hybrid nanoparticles modified with β-cyclodextrin, Appl. Surf. Sci. 305 (2014) 267–273.
[14] B. Zargar, H. Parham, A. Hatamie, Fast removal and recovery of amaranth by modified iron oxide magnetic nanoparticles, Chemosphere 76 (2009) 554–557.
[15] L. Zhou, C. Gao, W. Xu, Magnetic dendritic materials for highly efficient adsorption of dyes and drugs, ACS Appl. Mater. Interface 2 (2010) 1483–1491.
[16] X.L. Bao, Z.M. Qiang, W.C. Ling, J.H. Chang, Sonohydrothermal synthesis of MFe_2O_4 magnetic nanoparticles for adsorptive removal of tetracyclines from water, Sep. Purif. Technol. 117 (2013) 104–110.
[17] T.X. Fan, S.K. Chow, D. Zhang, Biomorphic mineralization: From biology to materials, Prog. Mater. Sci. 54 (2009) 542–659.
[18] W. Water, S.Y. Chu, Y.D. Juang, S.J. Wu, Li_2CO_3-doped ZnO films prepared by RF magnetron sputtering technique for acoustic device application, Mater. Lett. 57 (2002) 998–1003.
[19] N. Kannan, M.M. Sundaram, Kinetics and mechanism of removal of methylene blue by adsorption on various carbons—A comparative study, Dyes Pigm. 51 (2001) 25–40.
[20] Y.S. Ho, G. McKay, Pseudo-second order model for sorption processes, Process Biochem. 34 (1999) 451–465.
[21] I. Langmuir, The adsorption of gases on plane surfaces of glass, mica and platinum, J. Am. Chem. Soc. 40 (1918) 1361–1403.
[22] H.M.F. Freundlich, Uber die adsorption in losungen, Z. Phys. Chem. 57 (1906) 385–470.
[23] R. Rahimi, H. Kerdari, M. Rabbani, M. Shafiee, Synthesis, characterization and adsorbing properties of hollow Zn-Fe_2O_4 nanospheres on removal of Congo red from aqueous solution, Desalination 280 (2011) 412–418.
[24] B. Cheng, Y. Le, W.Q. Cai, J.G. Yu, Synthesis of hierarchical $Ni(OH)_2$ and NiO nanosheets and their adsorption kinetics and isotherms to Congo red in water, J. Hazard. Mater. 185 (2011) 889–897.
[25] C. Wang, Y. Le, B. Cheng, Fabrication of porous ZrO_2 hollow sphere and its adsorption performance to Congo red in water, Ceram. Int. 40 (2014) 10847–10856.
[26] H.M. Zhu, M.M. Zhang, Y.Q. Liu, L.J. Zhang, R.P. Han, Study of congo red adsorption onto chitosan coated magnetic iron oxide in batch mode, Desal. Water Treat. 37 (2012) 46–54.
[27] S. Karagoz, T. Tay, S. Ucar, M. Erdem, Activated carbons from waste biomass by sulfuric acid activation and their use on methylene blue adsorption, Bioresour. Technol. 99 (2008) 6214–6222.
[28] N. Mahmoodi, B. Hayati, M. Arami, C. Lan, Adsorption of textile dyes on Pine Cone from colored wastewater: Kinetic, equilibrium and thermodynamic studies, Desalination 268 (2011) 117–125.
[29] P. Baskaralingam, M. Pulikesi, D. Elango, V. Ramamurthi, S. Sivanesan, Adsorption of acid dye onto organobentonite, J. Hazard. Mater. 128 (2006) 138–144.